Journal of Biomedical Optics

SPIEDigitalLibrary.org/jbo

Second harmonic generation polarization properties of myofilaments

Masood Samim
Nicole Prent
Daniel Dicenzo
Bryan Stewart
Virginijus Barzda

SPIE

Journal of Biomedical Optics 19(5), 056005 (May 2014)

Second harmonic generation polarization properties of myofilaments

Masood Samim,[a,b,†] Nicole Prent,[a,b,†] Daniel Dicenzo,[b] Bryan Stewart,[c] and Virginijus Barzda[a,b,*]
[a]University of Toronto, Department of Physics and Institute for Optical Sciences, 60 Saint George Street, Toronto, Ontario M5S1A7, Canada
[b]University of Toronto Mississauga, Department of Chemical and Physical Sciences, 3359 Mississauga Road North, Mississauga, Ontario L5L1C6, Canada
[c]University of Toronto Mississauga, Department of Biology, 3359 Mississauga Road North, Mississauga, Ontario L5L1C6, Canada

Abstract. Second harmonic generation (SHG) polarization microscopy was used to investigate the organization of myosin nanomotors in myofilaments of muscle cells. The distribution of the second-order nonlinear susceptibility component ratio $\chi^{(2)}_{zzz}/\chi^{(2)}_{zxx}$ along anisotropic bands of sarcomeres revealed differences between the headless and head-containing regions of myofilaments. The polarization-in polarization-out SHG measurements of headless myosin mutants of indirect flight muscle in *Drosophila melanogaster* confirmed a lower susceptibility component ratio compared to the head-containing myocytes with wild-type myosins. The increase in the ratio is assigned to the change in the deflection angle of the myosin S2 domain and possible contribution of myosin heads. The nonlinear susceptibility component ratio is a sensitive indicator of the myosin structure, and therefore, it can be used for conformational studies of myosin nanomotors. The measured ratio values can also be used as the reference for *ab initio* calculations of nonlinear optical properties of different parts of myosins. [DOI: 10.1117/1.JBO.19.5.056005]

Keywords: muscle myosin; heavy meromyosin; nonlinear susceptibility ratio; second harmonic generation microscopy.

Paper 140086R received Feb. 13, 2014; revised manuscript received Mar. 24, 2014; accepted for publication Apr. 11, 2014; published online May 7, 2014.

1 Introduction

The structure of muscle myosin within a sarcomere can be characterized with the second harmonic generation (SHG) microscopy.[1–5] SHG is generated in myofilaments that contain myosin molecules organized in a cylindrically symmetric structure.[6,7] Various conformational states of the myosin molecules influence the SHG polarization properties during muscle contraction. Therefore, understanding the structural basis of SHG signal is of paramount importance in order to employ the SHG polarization microscopy for muscle contractility studies.

The *ab initio* calculations can be performed to model polarization properties of SHG generated from fibrillar proteins.[8,9] The calculated susceptibility values have to be compared with the experimental results, which requires measurements of SHG polarization properties of structural domains constituting the protein. The myosin molecules are composed of the light meromyosin (LMM) domains that constitute the core of the myofilaments, whereas the heavy meromyosin (HMM) regions act as mobile parts to produce a power stroke when attached to actin filaments during muscle contraction. The LMM domains can be studied in the central region of anisotropic bands (A-bands) of sarcomeres, where the myofilaments do not contain myosin heads, or in mutants lacking myosin head domains. By understanding polarization properties of LMM domains, the SHG polarization contribution of myosin heads and S2 domains during myocyte contraction can be estimated.

SHG polarization measurements can be performed by measuring the signal intensity at multiple laser polarization orientations.[1,2,6] When small variations in polarization properties are of interest or high precision measurements are required, an analyzer can be added to perform the polarization-in polarization-out (PIPO) SHG experiments.[10,11] PIPO SHG measurements render a two-dimensional surface that can be fit with the theoretical model to obtain the susceptibility ratio values and the orientation of the cylindrical axis of the myofibril.[10,11] The fitting, therefore, eliminates the uncertainty with the orientation of the polarizer with respect to the myofilament axis during measurements. In addition, the birefringence can be accounted for when fitting the PIPO data to obtain a more accurate susceptibility component ratio, $b = \chi^{(2)}_{zzz}/\chi^{(2)}_{zxx}$, as will be shown in this article.

This article will explore the variations of nonlinear susceptibility ratio b along the myofilaments in the anisotropic (A-) bands of sarcomeres. The investigation will also determine the b values of different myosin protein domains in indirect flight muscles (IFMs) of wild-type and myosin mutants of fruit flies. The results can be used to interpret the commonly reported molecular nonlinear susceptibility ratio values in terms of myosin molecular structures.

2 Material and Methods

2.1 *Sample Preparation*

Muscle samples from rats (*Rattus norvegicus*) and fruit flies (*Drosophila melanogaster*) were used in this study. Freshly culled rats, which were euthanized by CO_2 narcosis followed by cervical dislocation according to the ethically approved protocol, were obtained from the University of Toronto,

*Address all correspondence to: Virginijus Barzda, E-mail: virgis.barzda@utoronto.ca

†These authors contributed equally to the work presented here.

0091-3286/2014/$25.00 © 2014 SPIE

Mississauga Vivarium. After the rats were culled, the hind paws were removed and skinned to reveal the muscle tissues, and then soaked at a room temperature in 10% formaldehyde solution overnight. After the *in situ* fixing process, the hind paw was washed several times with fresh saline buffer [0.14-M NaCl, 0.01-M HEPES, 0.012-M Dextrose, 0.004-M $MgCl_2$, 0.001-M $CaCl_2$, pH 7.4], and the soleus muscles were excised using surgical forceps and scissors. For polarization experiments, a single fiber was gently isolated from the fixed tissue under a dissection microscope and placed between microscope coverslips. The soleus muscles from two animals were used for PIPO investigation. In total six PIPO data sets (three from each muscle) were acquired.

IFMs from two mutants, Mhc^{10}; Y97 (containing LMM and S2 domains) and Mhc^{10} (without myosin), and a wild-type of fruit fly were used in this study.[12] The Mhc^{10} lacks myosin and therefore shows a very weak-SHG signal. Thus, Mhc^{10} was used only as a reference measurement. An adult fruit fly was held in place by pins and dissected under the dissection microscope to extract IFMs. The IFMs were then fixed in a mixture of 4% formaldehyde and saline solution for 3 min.[4] Thin slices were cut and placed between two glass coverslips in the saline buffer for SHG-PIPO microscopy.

2.2 *Laser and Microscope Setup*

The details of the laser system and the microscope setup are described elsewhere.[10,13–15] Briefly, a $Yb:KGd(WO_4)_2$ laser oscillator was used for imaging, which produced a 430-fs pulsed beam at 1028-nm wavelength with a repetition rate of 14.3 MHz. The PIPO SHG microscope used a linearly polarized laser beam. A linear polarizer followed by a half-wave plate (HWP) placed on a rotation stage was inserted in front of the excitation objective to allow rotation of the laser beam polarization orientation. Light then passed through the 0.75-NA excitation objective and was focused on the sample. SHG generated in the forward direction was collected by a home-built objective. The focal volume point-spread-functions had full-width at half-maximums of about 460 ± 90 nm laterally and 2.8 ± 0.4 μm axially. The SHG polarization orientation was analyzed by a linear analyzer mounted on a rotation stage. The outgoing signal was filtered for the SHG wavelength with a BG39 and a 510 to 520-nm band-pass interference filter and detected with a photomultiplier tube (Hamamatsu, Bridgewater, New Jersey, model H7421-40).

2.3 *SHG PIPO Measurement and Analysis*

The SHG intensity images at different incoming beam polarization angles θ and analyzer angles φ were recorded to obtain the PIPO plots. For the fruit fly imaging, the HWP rotated the incoming field polarization 10 times at equal increments from 0 to 180 deg. At each polarization angle, θ, the analyzer was rotated by $\varphi = 18$ deg increments from 0 to 180 deg, and images were recorded for each combination of polarizer and analyzer angles. Incident laser intensities on the samples were optimized to keep signal degradation below a 10% variation during PIPO measurements. The signal degradation was monitored at every 11^{th} scan of the PIPO measurements, which were performed at $\theta = 0$ deg and $\varphi = 0$ deg of polarizer and analyzer positions, respectively. The acquired images were fit globally for each pixel with Eq. (1). For the rat muscle data, PIPO plots were obtained at seven equally incremented analyzer orientation angles for 13 (11 equally incremented and ± 45 deg) incident polarization angles from 0 to 180 deg inclusive. For each pixel, the SHG-PIPO surface plot was fit to Eq. (1) using custom MATLAB® scripts (Math Works, Natick, Massachusetts). These fits determined the b values for all pixels in the image. Since not all pixels in the PIPO images contain enough signals for fitting with Eq. (1), only pixels with well-fitted data of $R^2 > 0.95$ are considered. Histograms of the b values were then generated from the data that had $R^2 > 0.95$.

The SHG polarization intensity from a cylindrically symmetric sample at a particular laser polarization angle θ and an analyzer angle φ from the laboratory, Z-axis can be described according to the following equation (see Appendix for detailed derivation):

$$I_{2\omega}(\theta,\varphi) = I_B + C\{\sin^2\varphi \sin^2 2\theta + \cos^2\varphi[\sin^4\theta + \frac{1}{2} b \cos(2\delta_\omega)\sin^2 2\theta + b^2\cos^4\theta] + \sin 2\varphi \sin 2\theta(\cos\delta^- \sin^2\theta + b\cos\delta^+\cos^2\theta)\}, \quad (1)$$

where δ_ω and $\delta_{2\omega}$ are phase delays that incident and emitted signal experience due to birefringence in the sample, respectively, and $\delta^\pm = \delta_\omega \pm \delta_{2\omega}$. I_B and C are fitting parameters accounting for any background signal and the intensity amplitude, respectively. Kleinman symmetry is assumed in Eq. (1).[2,16] The ratio $b = \chi^{(2)}_{zzz}/\chi^{(2)}_{zxx}$ is sensitive to the molecular orientation distribution of SH scatterers within the focal volume. It is assumed that the cylindrical axis of the myofilament is oriented along the Z-axis and perpendicular to the X-axis, while the laser propagation direction is along Y-axis of the laboratory frame of reference. To reduce the number of free fitting parameters in Eq. (1), the background value, I_B was determined *a priori* and included as a fixed parameter. In addition, the birefringence phases were constrained, based on the measured thickness of the muscle fiber and the assumption that the birefringence, Δn, in muscle is $0.001 \leq \Delta n \leq 0.003$.[11,17] The two phase parameters were fit by setting initial phase values and variation boundaries estimated from the thickness of the myocyte and the position of the imaging plane. The path length estimates were made based on the three-dimensional images of the myocytes recorded with SHG and third harmonics generation (THG) microscopes. The best fit PIPO plots at each pixel of the image yield the b values, which can be displayed as the ratio value images.

3 Results and Discussion

3.1 *Spatial Variability of Susceptibility Component Ratio along Myofilament*

The nonlinear susceptibility ratio b value is expected to differ between the middle and the edges of A-bands due to headless central region and head-containing peripheral regions of the myofilaments. Indeed, the polarization SHG imaging with PIPO measurements was able to reveal the susceptibility component ratio differences along the filaments (Fig. 1). Alternating bright A- and dark isotropic (I-) bands are clearly visualized with SHG microscopy, as shown in Fig. 1(a), due to the nonzero second-order susceptibility of myosin filaments located in A-bands. The example SHG image in panel (a) is shown at specific polarizer and analyzer angles ($\theta = \pi/4$, $\varphi = 3\pi/10$). The PIPO plots for each pixel are assembled from many images

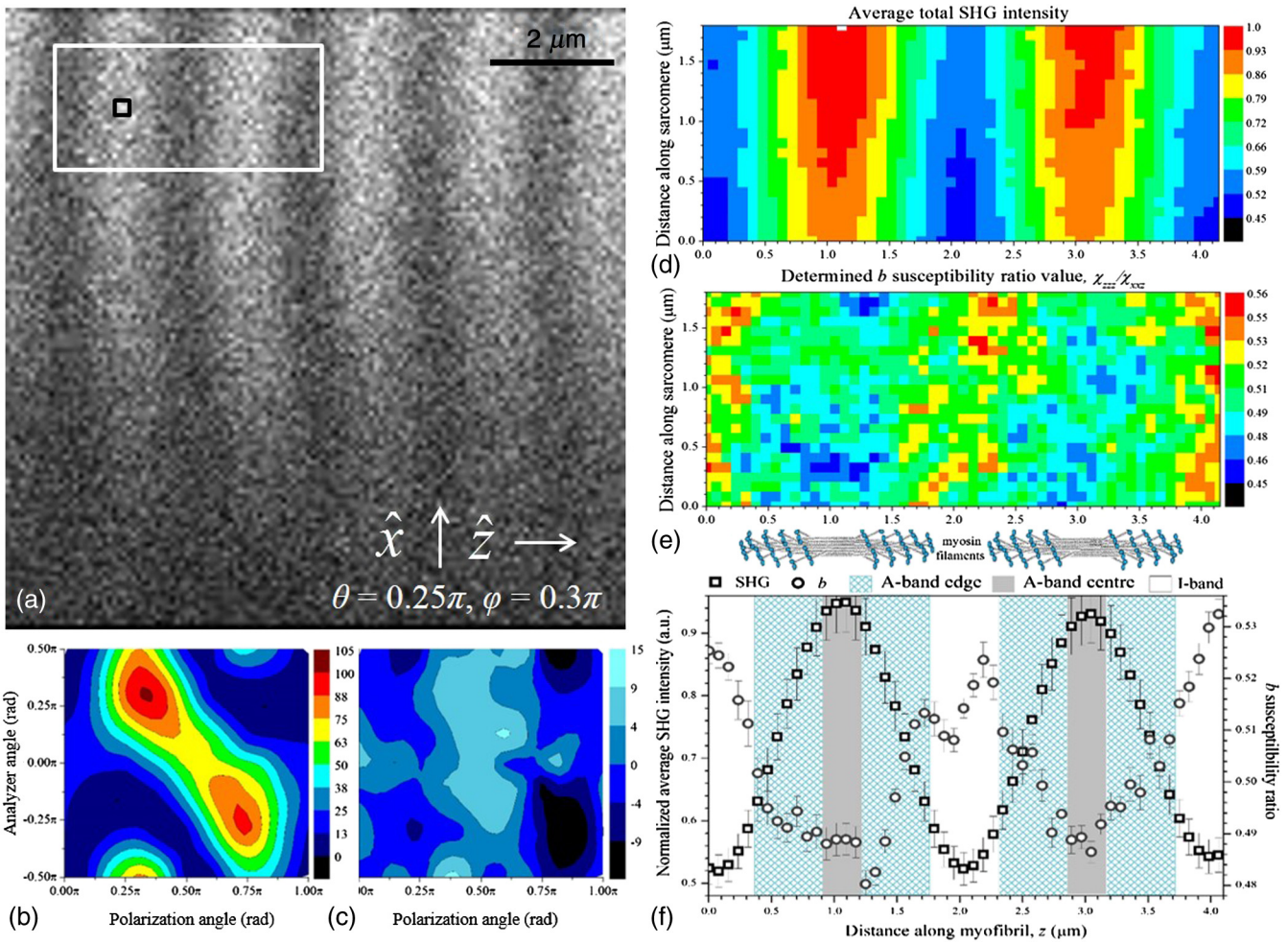

Fig. 1 Second harmonic generation (SHG) polarization dependence in rat myofibrils. SHG image (a) recorded at the polarization $\theta = 0.25\pi$ and analyzer $\varphi = 0.3\pi$ angles with respect to the indicated cylindrical z-axis. The small black square shows the region that corresponds to the experimental polarization-in polarization-out (PIPO) plot (b) and the PIPO best fit residual plot (c). The area indicated by the white rectangle in (a) is analyzed by fitting Eq. (1) to the experimental PIPO plots of each pixel in the area. The extracted SHG intensity amplitudes C [see Eq. (1)] and the determined b susceptibility ratios for each pixel are shown in (d) and (e), respectively. The SHG intensity amplitude is normalized to the highest value in panels (b) and (d). The mean SHG intensity and b values over the vertical axis in (d) and (e) is shown in (f) with error bars indicating the standard deviation over the vertical axis of the respective panel.

recorded at different combinations of laser polarization and analyzer orientation. The small square in panel (a) indicates the pixel from which the SHG PIPO plot is presented as an example in panel (b). The PIPO plot was fit with Eq. (1), and the residual plot is presented in the panel (c). Similar PIPO plots were fit for each 3×3 pixel area of the image. A 25×55 pixel region containing two sarcomeres was selected for the polarization analysis. The area [shown by the large rectangle in panel (a)] had a constant myosin fiber thickness of about 40 μm and was imaged at a depth of $\sim$30 μm within the fiber. PIPO data for each 3×3 pixel in the selected area (1219 pixels) were fit with Eq. (1). Spatial variations in the SHG intensity amplitude C and the determined susceptibility ratio values b for two A-bands of sarcomeres from the SHG image in Fig 1(a) are shown in panels (d) and (e), respectively.

The distribution of ratio b values in Fig. 1(e) gives a few important observations: At the center of the myosin thick filament (M-line), the b value is lower compared with the edges of the A-band $[t(822) = -7.46, p < 0.001]$. Interestingly, I-bands and edges of A-bands have higher b values than M-lines. The difference of the mean b values between the I-bands and A-band is also significant $[t(1033) = 20.21, p < 0.001]$. On average, b values from the regions corresponding to M-lines are 0.489 ± 0.001 (mean $\pm$ standard error), whereas at the edges of A-bands are 0.498 ± 0.001 and regions corresponding to I-bands show 0.519 ± 0.001.

The anti-correlation analysis between the SHG intensity and the determined b value, calculated as the average Pearson's correlation coefficient $\bar{p}(I_{2\omega}, b) = -0.66 \pm 0.03$ between panels (d) and (e), also implies that the b values are lower at the center of A-bands (higher SHG intensity), corresponding to the M-line.

It should be noted that although the differences between the average b values at the center of the myosin filaments, compared to the values at the edges are small ($\sim$2%), they can be distinguished by SHG-PIPO microscopy, and, therefore, b values can be potentially used for studying conformational changes in myosin molecules at different contraction states of sarcomeres. The results suggest that b values are different for the HMM and

LMM domains of the myosin molecule. Hence, additional experiments were performed to investigate the variation of the susceptibility component ratio for the headless part of the myosin.

The central M-line region consists of mainly the antiparallel LMM domain and contains no myosin heads. In contrast, edges of A-bands and I-bands have a higher proportion of the HMM domain and have lower SHG intensity. The SHG detected in the I-band is most likely from the HMM groups at the ends of the myosin filaments that convolve with the edge of focal volume during the raster scanning. To either side of the central region in the myosin filament, the myosin molecules are arranged along the filament with the HMM groups deflected away from the central filament axis. Assuming that myosin molecules are cylindrically organized in the myosin filament, the b value acts as a measure of the effective orientation distribution of the nonlinear dipoles in the filament.[2,10,18,19] If helical domains have hyperpolarizability ratio values below 3, an increase in the deviation angle of the helical domains from the cylindrical axis results in higher measured b values.[10,20] This measured distribution of the b values in the A-band is in agreement with the structure of the myosin filament, where the α-helices of the LMM in the bare region are aligned along the myofilament, while the orientation of α-helices in S1 and S2 domains of the HMM deviates from the cylindrical axis of the filament.

3.2 *Headless Myosin Mutant Imaging*

The fruit fly mutant Mhc^{10}; Y97[4,12] was imaged with SHG-PIPO microscopy and compared with data from intact sarcomeres of the wild-type IFMs (Fig. 2). The mutant Mhc^{10} does not contain myosin, and therefore the SHG signal was absent from the sarcomeres[4] (data not shown). The myosin of IFM in the Mhc^{10}; Y97 fly is mutated twice, once to eliminate the myosins and then to add headless myosin filaments. A previous study of the mutants had found that the mutant Mhc^{10}; Y97 retained the myosin heavy chain, the rod, and the regulatory light chain (located on the neck of the S1 region).[12] The previous results also showed that the Mhc^{10}; Y97 mutants were only missing the globular heads.[4,12]

Figures 2(b) and 2(g) show the SHG images of the wild-type and Mhc^{10}; Y97 IFMs that were acquired for the purpose of PIPO analyses, respectively. The wild-type myocyte structures generated the highest SHG signal and also demonstrated the familiar striation patterns with easily distinguishable A- and I-bands. In contrast, Mhc^{10}; Y97 mutant tissue generated less SHG intensity compared to the wild-type and also had irregular sarcomere structures that appear like splotches. The irregular SHG intensity patterns from Mhc^{10}; Y97 samples highlight the organizational role of myosin heads in the structure of a sarcomere. Although the A-bands are visible, the striated patterns are not obvious in the image of the mutant. Moreover, the I-bands are difficult to visualize within the image. The lack of myosin heads disrupts the typical sarcomere formation and results in a distorted SHG image. The SHG imaging is consistent with the previous study of the mutants, which showed that as the level of mutation increases, the crystalline structure of the sarcomeric myosin becomes more affected.[4,12]

Susceptibility component ratio maps provide further details about the structure of A-bands [Figs. 2(c) and 2(h)]. SHG-PIPO analyses of the wild-type muscle structure revealed an average b value of 0.60 ± 0.10 and a relatively broad distribution that extends to the higher ratio values [Fig. 2(d)]. In contrast, the mutant Mhc^{10}; Y97 showed an average b value of 0.45 ± 0.05, and the distribution of the ratio was narrower and significantly different than the wild-type sample [$t(5546) = -62.88$, $p < 0.0001$; Figs. 2(d) and 2(i)]. The narrow ratio distribution in the muscle mutant is surprising since the muscle fiber structure in SHG images appears much more distorted compared with the wild type. This is in contrast to findings of collagen fiber distributions in various tissue. In a rat-tail tendon with

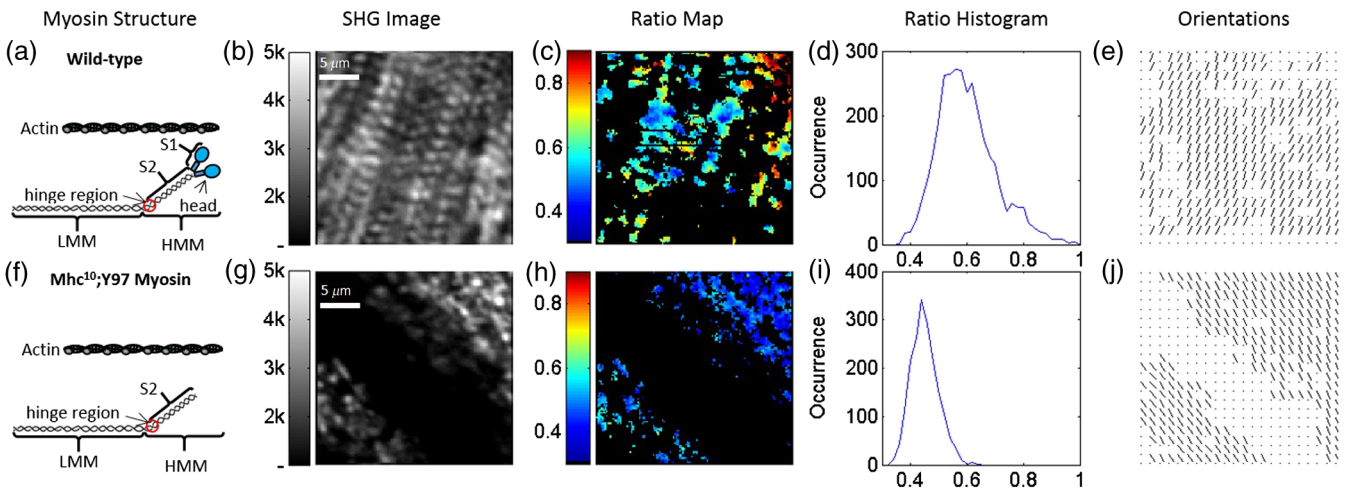

Fig. 2 SHG-PIPO analyses of wild-type (a to e) and mutant (f to j) of indirect flight muscles in the *Drosophila melanogaster*. Diagrams of wild-type (a) and Mhc;Y97 mutant (f) of myosin with indicated S1, S2, light meromyosin (LMM), and heavy meromyosin (HMM) domains. SHG images acquired for the PIPO analyses (25×25 μm^2 area) of wild-type (b) and the mutant (g) of IFM are shown. A color map indicating the ratio b values for wild type (c) and the mutant (h) with fits at $R^2 > 0.95$. Histogram of the b ratios for wild type (d) and the mutant (i) obtained from the images (c) and (h), respectively. The average ratio for the wild type is 0.60 ± 0.10 and for the mutant is 0.45 ± 0.05. Vector plots indicating the direction of myofibrils in the sarcomeres for the wild type (e) and the mutant (j), respectively.

regular and straight collagen fibers, a narrow distribution and small average b ratio value are observed. In comparison, in dermis, cornea, or bone with a relatively irregular distribution of collagen fibers, a broader distribution and larger b ratio values are found.[10] The narrow distribution indicates a uniform myosin structure along myofilaments in the mutated sarcomeres, which is expected from a homogenous myosin rod domain.

Wild-type muscles have fully intact myosin proteins that allow the myosin to attach to the actin filaments. The attachment alters the myosin head and S2 domain deflection angles from the myofilament axis and leads to an increase in the susceptibility component ratio [Fig. 1(d)].[21] The observed b values represent the ratio of second harmonic generated from myosin molecules that are embraced in a single-focal volume. The ratio is determined by several factors including the ratios of different parts of the myosin molecule, the conformational states of myosin (attached, detached, or intermediate state of myosin), and the tilt of a myofibril with respect to the image plane. From the ratio image (Fig. 2), it is visible that the heterogeneity is present on a single-sarcomere level and also between sarcomeres, as well as in different areas of the myocyte. The distribution of the ratio in the wild-type sample is large, ranging from 0.3 to 0.9, indicating that the sample contains myosins in attached and detached states. The lower ratio found in the Mhc^{10}; Y97 sample could be due to both: the lack of myosin head domains and a reduced variation in the deflection angle of the S2 region. Most probably, the S2 domain has significant influence on the ratio due to the ordered helical structure rendering larger contribution to the SHG signal. In Mhc^{10}; Y97, due to the inability of the myosin to attach to actin, the S2 region may have a lower deflection angle from the myofilament axes resulting in lower measured b values. This also explains the narrow ratio distribution in the histogram [Fig. 1(h)], pointing to a uniform orientation of the S2 domains.[10] The significant influence of S2 domains on the measured b values can be helpful for studies of myosin nanomotor conformational changes during muscle contractions. The rapid SHG polarization changes occurring during muscle contraction can be probed with advanced orthogonally polarized multibeam microscopy.[22] The low b values for the mutant Mhc^{10}; Y97 and the M-line of the wild-type myocyte indicates that LMM with detached S2 domain has the susceptibility ratio of $0.45 < b < 0.49$. This ratio can be used as an experimental value for *ab initio* calculations of the nonlinear susceptibility of the myosin helical domains.

4 Conclusion

SHG polarization microscopy provides evidences that the susceptibility component ratio value of headless myosins arranged in the myofilament is $0.45 < b < 0.49$. In contrast, the head containing regions of myofilaments give higher values of the susceptibility component ratio. The broad distribution of the ratio shows that conformational states of attached and detached myosin heads and the variation in the deflection angle of the S2 domain influence the susceptibility component ratio. Thus, the ratio can be used for dynamic studies of contracting myocytes. The determined ratio of LMM with S2 domain can be potentially used for *ab initio* calculations to model nonlinear properties of myosin. In summary, the SHG PIPO imaging technique provides a robust and precise basis for studies of conformational dynamics of myosins within the A-bands of sarcomeres during a muscle contraction.

Appendix

A nonlinear optical polarization $P_{2\omega}$ is proportional to the second-order susceptibility tensor, $\chi^{(2)}$ and the square of the incident electric field E_ω, according to the following relation:[6]

$$\begin{bmatrix} P_{2\omega,x} \\ P_{2\omega,z} \end{bmatrix} = 2\varepsilon_0 \begin{bmatrix} 2\chi^{(2)}_{xxz} E_{\omega,x} E_{\omega,z} \\ \chi^{(2)}_{zxx} E^2_{\omega,x} + \chi^{(2)}_{zzz} E^2_{\omega,z} \end{bmatrix}, \tag{2}$$

where ε_0 is the permittivity of free space, and xyz are the molecular frame of reference. In SHG-PIPO microscopy, the incident electric field polarization is rotated by the angle θ, and the outgoing response signal is passed through a linear analyzer oriented at an angle φ with respect to the laboratory Z-axis. The measured SHG intensity is then characterized by the relation:

$$\begin{aligned} I_{2\omega}(\theta,\varphi) &\propto |\sin\varphi P_{2\omega,x} + \cos\varphi P_{2\omega,z}|^2 \\ &\propto [\sin\varphi \sin(2\theta) + \cos\varphi(a\sin^2\theta + b\cos^2\theta)]^2, \end{aligned} \tag{3}$$

where $a = \chi^{(2)}_{zxx}/\chi^{(2)}_{xxz}$ and $b = \chi^{(2)}_{zzz}/\chi^{(2)}_{xxz}$, and the ratio $a = 1$ when Kleinman symmetry holds (i.e., the susceptibility ratio is wavelength-independent). It is assumed that the cylindrical axes of the myofibrils are oriented along the Z-axis, while propagation of the beam is along the Y-axis of the laboratory frame of reference. If an incident beam experiences a phase delay δ_ω due to birefringence, the components of the incident electric field in Eq. (2) can be substituted with $E_{\omega,x} = E_0 \sin\theta$ and $E_{\omega,z} = E_0 e^{-i\delta_\omega} \cos\theta$, therefore:

$$\begin{aligned} I_{2\omega}(\theta,\varphi) = I_B + C|&\sin\varphi \sin(2\theta) e^{-i\delta_\omega} \\ &+ \cos\varphi(a\sin^2\theta + b e^{-i2\delta_\omega}\cos^2\theta) e^{-i\delta_{2\omega}}|^2, \end{aligned} \tag{4}$$

where $\delta_{2\omega}$ is the induced phase of the emitted second-harmonic field due to birefringence. I_B and C are fitting constants accounting for any background signal and SHG intensity amplitude, respectively.

Acknowledgments

This work was supported by grants from the Natural Sciences and Engineering Research Council of Canada and the Canadian Institutes of Health Research. Mutant stocks were kindly provided by Professor S. Bernstein from San Diego State University.

References

1. V. Nucciotti et al., "Probing myosin structural conformation in vivo by second-harmonic generation microscopy," *Proc. Natl. Acad. Sci.* **107**(17), 7763–7768 (2010).
2. S. Plotnikov et al., "Characterization of the myosin-based source for second-harmonic generation from muscle sarcomeres," *Biophys. J.* **90**(2), 693–703 (2006).
3. N. Prent et al., "Inter myofilament dynamics of myocytes revealed by second harmonic generation microscopy," *J. Biomed. Opt.* **13**(4), 041318 (2008).
4. C. Greenhalgh et al., "Influence of semicrystalline order on the second-harmonic generation efficiency in the anisotropic bands of myocytes," *Appl. Opt.* **46**(10), 1852–1859 (2007).
5. M. Samim et al., "Three-dimensional video-rate nonlinear microscopy of contracting myocytes," *Eur. Biophys. J. Biophys.* **40**(1 Supp.), 122–122 (2011).

6. S.-W. Chu et al., "Studies of $\chi(2)/\chi(3)$ tensors in submicron-scaled bio-tissues by polarization harmonics optical microscopy," *Biophys. J.* **86**(6), 3914–3922 (2004).
7. F. Vanzi et al., "New techniques in linear and non-linear laser optics in muscle research," *J. Muscle Res. Cell Motil.* **27**(5–7), 469–479 (2006).
8. A. Tuer et al., "Nonlinear multicontrast microscopy of hematoxylin-and-eosin-stained histological sections," *J. Biomed. Opt.* **15**(2), 026018 (2010).
9. A. Tuer et al., "Three-dimensional visualization of the first hyperpolarizability tensor," *J. Comput. Chem.* **32**(6), 1128–1134 (2011).
10. A. E. Tuer et al., "Hierarchical model of fibrillar collagen organization for interpreting the second-order susceptibility tensors in biological tissue," *Biophys. J.* **103**(10), 2093–2105 (2012).
11. N. Prent et al., "Polarisation-in polarisation-out second-harmonic generation microscopy in Birefringent biological structures," in *Proc. Int. School of Physics "Enrico Fermi": Microscopy Applied to Biophotonics*, F. S. Pavone, P.T.C. So, and P.M.W. French, Eds., IOS Press, Varenna, Italy (2013).
12. R. M. Cripps, J. A. Suggs, and S. I. Bernstein, "Assembly of thick filaments and myofibrils occurs in the absence of the myosin head," *EMBO J.* **18**(7), 1793–1804 (1999).
13. D. Sandkuijl et al., "Differential microscopy for fluorescence-detected nonlinear absorption linear anisotropy based on a staggered two-beam femtosecond Yb:KGW oscillator," *Biomed Opt Express* **1**(3), 895–901 (2010).
14. A. Major, D. Sandkuijl, and V. Barzda, "A diode-pumped continuous-wave Yb:KGW laser with N-g-axis polarized output," *Laser Phys. Lett.* **6**(11), 779–781 (2009).
15. A. Major, D. Sandkuijl, and V. Barzda, "Efficient frequency doubling of a femtosecond Yb:KGW laser in a BiB3O6 crystal," *Opt. Express* **17**(14), 12039–12042 (2009).
16. M. Both et al., "Second harmonic imaging of intrinsic signals in muscle fibers in situ," *J. Biomed. Opt.* **9**(5), 882–892 (2004).
17. S. M. Baylor and H. Oetliker, "Birefringence signals from surface and T-System membranes of frog single muscle-fibers," *J. Physiol.-London* **264**(1), 199–213 (1977).
18. F. Tiaho, G. Recher, and D. Rouede, "Estimation of helical angles of myosin and collagen by second harmonic generation imaging microscopy," *Opt. Express* **15**(19), 12286–12295 (2007).
19. F. Vanzi et al., "Protein conformation and molecular order probed by second-harmonic-generation microscopy," *J. Biomed. Opt.* **17**(6), 060901 (2012).
20. A. Leray et al., "Organization and orientation of amphiphilic push-pull chromophores deposited in Langmuir-Blodgett monolayers studied by second harmonic generation and atomic force microscopy," *Langmuir* **20**(19), 8165–8171 (2004).
21. A. E. Tuer et al., "Nonlinear optical properties of type I collagen fibers studied by polarization dependent second harmonic generation microscopy," *J. Phys. Chem.B* **115**(44), 12759–12769 (2011).
22. M. Samim et al., "Differential polarization nonlinear optical microscopy with adaptive optics controlled multiplexed beams," *Int. J. Mol. Sci.* **14**(9), 18520–18534 (2013).

Biographies of the authors are not available.